Chapter 2

Hydrophobic Forces in the Foam Films Stabilized by Sodium Dodecyl Sulfate: Effect of Electrolyte

Abstract

Further studies of the hydrophobic force in foam films were carried out, including the effect of added inorganic electrolyte. We used a thin film balance of Scheludko-Exerowa type to obtain the disjoining pressure isotherms of the foam films stabilized by 10^{-4} M sodium dodecyl sulfate (SDS) in varying concentrations of sodium chloride (NaCl). The results were compared with the disjoining pressure isotherms predicted from the extended Derjaguin-Landau-Verwey-Overbeek theory, which considers contributions from hydrophobic force in addition to those from double-layer and van der Waals dispersion forces. The double layer forces were calculated from the surface potentials (ψ_s) obtained using the Gibbs adsorption equation and corrected for counterion binding effect, while the dispersion forces were calculated using the Hamaker constant (A_{232}) of 3.7×10^{-20} J. The hydrophobic forces were calculated from the equilibrium film thickness as described previously. The predicted disjoining pressure isotherms were in good agreement with the experimental ones. It was found that the hydrophobic force is dampened substantially by the added electrolyte.

10.1021/la048672g © 2004 American Chemical Society
Published on Web 11/18/2004

2.1 Introduction

Many investigators studied the stability of foams by measuring the disjoining pressures in free films (or between two air bubbles). If the pressure is positive the film and hence the foam is stable, and if the pressure is negative the foam is destabilized. The disjoining pressures can be measured using the thin-film balance (TFB) technique (1-3). Most the measurements were conducted with stable foam films at surfactant concentrations close to critical micelle concentrations (cmc). The results obtained under these conditions can be readily explained by the DLVO theory, according to which the disjoining pressure is due to double layer and van der Waals forces (4,5). In many industrial applications, however, foams are produced at much lower surfactant concentrations, in which case hydrophobic force may play a role. For example, the amount of surfactants used for froth flotation is 2 to 3 orders magnitudes lower than cmc.

Wetting films formed on a hydrophobic surface rupture spontaneously. The rupture thickness increases with increasing hydrophobicity of the solid. It was, therefore, suggested that air bubbles may be hydrophobic (6). Craig et al (7) measured the coalescence rate of gas bubbles in water in the presence of various electrolytes. They showed that bubble coalescence decreases with increasing electrolyte concentration, which suggests that hydrophobic force increases with decreasing electrolyte concentration. Craig et al. noted that van der Waals force alone can not counterbalance the hydrodynamic repulsion between air bubbles and, therefore, it is necessary to assume the presence of a stronger attractive force. Deschenes et al (8) showed that coalescence of gas bubbles is a sensitive probe of hydrophobic forces.

Recent TFB studies also showed evidence for the presence of hydrophobic force in soap films. Yoon and Aksoy (9) measured equilibrium film thicknesses of the foam films stabilized by dodecylaminine hydrochloride and calculated contributions from the hydrophobic force. They showed that the hydrophobic force increases with decreasing surfactant concentration. A problem in estimating the magnitude of hydrophobic force is that it depends critically on the double layer potentials calculated from Gibbs adsorption equation and corrected for the adsorption of counterions in the Stern layer. To minimize the errors in calculating the double layer potentials, Angarska, et al (10) calculated the contributions from hydrophobic force from the rupture thicknesses measured at 0.3 M NaCl, where double layer potential approaches zero. They still found the presence of strong hydrophobic forces, whose decay lengths are comparable to those measured between macroscopic hydrophobic solids.

In the present work, TFB studies were conducted to study the role of hydrophobic force in the stability of thin aqueous films. The measurements were conducted in the presence of sodium dodecyl sulfate (SDS) and NaCl. Initially, equilibrium film thicknesses were measured to determine the magnitudes of the hydrophobic forces at different SDS and NaCl concentrations. The method is similar to that described previously (9), except that double layer potentials were calculated using a counterion binding model developed in the present work. The hydrophobic force constants determined from the equilibrium film thickness were then used to fit the disjoining pressure isotherms obtained in the present work. The results will be used to discuss the role of electrolytes in the stability of foam films.

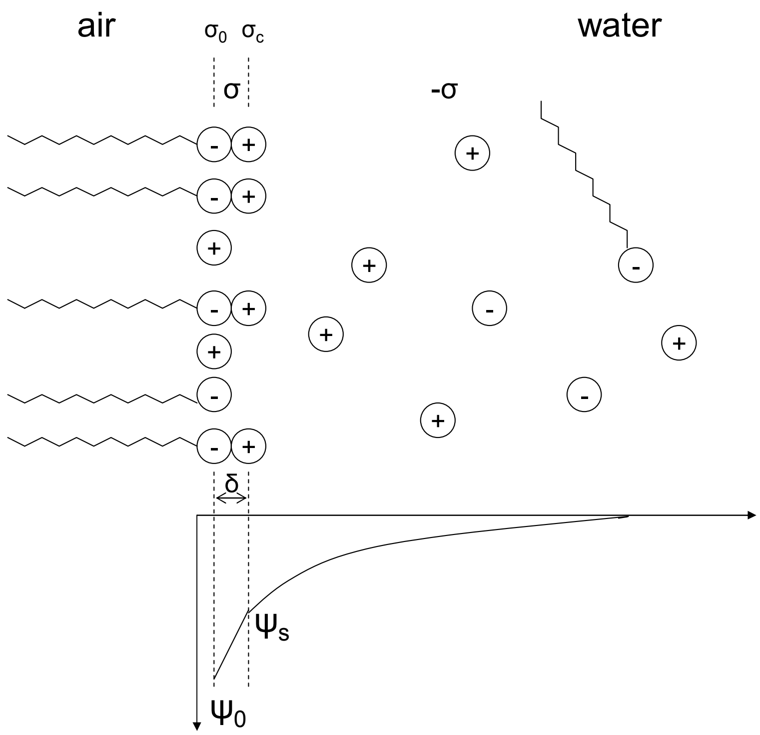

Figure 2.1 Schematic presentation of the electrical double-layer at the air-water interface. Anionic surfactants such as DS^- ions congregate at the air/water interface according to the Gibbs adsorption equation, creating a charge density of σ_0. Counter ions such as Na^+ ions adsorb on the charged surface, forming a Stern layer, with a charge density of σ_c. The distance between the two charged species is δ (=0.5 nm for the present system). Some counter ions penetrate the Stern layer. σ (=σ_0-σ_c) represents the net charge density at the Stern layer, which is counter-balanced by the charge-density ($-\sigma$) in the diffuse layer. ψ_0 and ψ_s are the surface and Stern potentials, respectively.

2.2 Counterion binding model

Figure 2.1 presents a counterion binding model for the SDS-NaCl system considered in the present work. Dodecyl sulfate (DS^-) ions adsorb at the air/water interface, and counterions (Na^+) form Stern layer. The charge density of at the locus of the polar heads of the DS^- ions is σ_0, and the charge density at the Stern layer is σ_c. Some of the counterions are shown to penetrate the Stern layer. The net charge density, σ (=σ_0-σ_c), in the Stern layer should be counterbalanced by the charge density in the diffuse layer $-\sigma$.

The formation of a single foam film represents essentially a process of approaching an air/water interface to another. When the two interfaces approach each other within the distance of approximately 100 nm, the adsorption density may change with separation. At low surfactant (or electrolyte) concentrations, however, the changes may be very small (less than 1%) according to Krustev and Müller's work (11). In such cases, one can use the charge densities calculated from the surface tension data using the Gibbs adsorption equation. Yaros et al. (12) showed that the charge densities obtained using the surface tension data are close to those obtained using the film conductance method.

The Gibbs surface excess (Γ_S) for the DS^- ions in the presence of an electrolyte (e.g., NaCl) can be calculated using the following relation (13):

$$\Gamma_s = -\frac{d\gamma}{nRTd\ln C_{SDS}} \tag{2.1}$$

where γ is surface tension, C_{SDS} the concentration of SDS, R the gas constant, T is the absolute temperature, and

$$n = \frac{2C_{SDS} + C_{NaCl}}{C_{SDS} + C_{NaCl}} - \frac{1.17C_{SDS}}{\sqrt{C_{SDS} + C_{NaCl}}}. \tag{2.2}$$

In the absence of NaCl, n approaches 2, while it approaches 1 in excess of salt.

At low surfactant concentrations, we may assume that SDS molecules are fully dissociated at the interface, in which case the surface charge density (σ_0) can be calculated using the following relationship (9,14):

$$\sigma_0 = eN_0\Gamma_S \tag{2.3}$$

where e is the electronic charge and N_0 Avogadro's number. One can then calculate the apparent surface potential (ψ_0) using the Grahame equation (15):

$$\sigma_0 = \sqrt{8kT\varepsilon_0\varepsilon_r n_0}\,\sinh\left(\frac{e\psi_0}{2kT}\right), \tag{2.4}$$

where ε_0 and ε_r are the permittivity of vacuum and the dielectric constant of water, respectively, k Boltzmann's constant, and n_0 is the number density of electrolyte.

After obtaining the apparent surface potential (ψ_0) by using the Poisson-Boltzmann approximation, one can also calculate the Stern potential (ψ_s) in a manner similar to the model developed by Warszynski et al (16).

The net charge density (σ) in the Stern layer is given by the following relationship:

$$\sigma = \sigma_0 - \sigma_c = eN_0(\Gamma_s - \Gamma_c) \tag{2.5}$$

where Γ_c is the surface excess of the counterions in the Stern layer. One can calculate the Stern potential ψ_s from σ once again using the Grahame equation:

$$\sigma = \sqrt{8kT\varepsilon_0\varepsilon_r n_0}\,\sinh\left(\frac{e\psi_s}{2kT}\right) \tag{2.6}$$

Substituting Eq. [2.6] to the following relationship:

$$\psi_0 = \psi_s + \frac{\sigma\delta}{\varepsilon_0 \varepsilon_s} \qquad [2.7]$$

where ε_s is the local dielectric constant in the Stern layer and δ is the distance between the polar head of DS^- ion and Na^+ ion in the Stern layer, one obtains the following:

$$0.2078\sqrt{C_{SDS} + C_{NaCl}}\,\sinh(19.489\psi_s) + \psi_s - \psi_0 = 0 \qquad [2.8]$$

which can be used to obtain the values of ψ_s from ψ_0 (using Eqs. [2.1-2.3], SDS concentration (C_{SDS}) and NaCl concentration (C_{NaCl}). The constants of Eq. [2.8] have been obtained from T=25^{o}C, ε_s=32 (17), and δ=0.5 nm. The value of δ is somewhat arbitrary. However, the changes in ψ_s are within 5 mV as δ varies from 0.3 to 0.7 nm at low electrolyte concentrations.

2.3 Experimental Section

2.3.1 Materials

Specially pure sodium dodecyl sulfate (SDS) was obtained from BDH and recrystallized from ethanol. Its surface tension isotherm showed no minimum near cmc, indicating that the surfactant has no significant impurities. A Nanopure water treatment unit was used to obtain double-distilled and deionized water with a conductivity of 18.2 MΩ·cm-1. A high-purity sodium chloride (99.99%) from Alfa Aesar was used as an electrolyte.

2.3.2 Experimental Method

Surface tension

The surface tensions were determined by the pendant drop method, utilizing a surface tension/contact angle meter, FTÅ 125, from First Ten Ångstroms. All the solutions were prepared at least one day before experiment and used within one week to minimize the hydrolysis effect.

Film thickness and disjoining pressure

The thin film balance (TFB) technique developed by Scheludko and Exerowa[1] was used to measure the thickness of soap films. The TFB cell was placed on a tilt stage (M-044.00, Polytec PI), which was mounted on an inverted microscope stage (Olympus IX51). The cell was water-jacketed to maintain the temperature at 25±0.1°C. The film thickness was measured by passing the white light reflected from a foam film through a band-pass filter (LCS10-546, Laser components). The light intensities were measured by means of a photosensor (H5784, Hamamastsu) equipped with a power supply (C7169, Hamamastsu). The fluorescence condenser of the microscope was modified so that the illuminated area of the film was small and, hence, can better probe the plane-parallel regions of the film. The film thickness was calculated online using a data-acquisition hardware and a homemade software.

Scheludko cells with 1.0 and 2.0 mm radii were used to measure the disjoining pressures below 150 Pa, while a bike-wheel microcell (18) with a hole diameter of 0.75 mm was used to measure the disjoining pressure above 150 Pa. The bike-wheel film holder was reusable, had a uniform liquid drainage inside, and exhibited an air/water entry pressure of about 10 KPa. The working equation for the measurement of disjoining pressure is (19):

$$\Pi = P_g - P_r + \frac{2\gamma}{r} - \Delta\rho g h_c \qquad [2.9]$$

where P_g is the pressure in the cell, P_r the external reference pressure, r the radius of the capillary tube, $\Delta\rho$ the density difference between the aqueous solution and air, g the gravitational constant, and h_c is the height of aqueous column in the capillary tube above the film.

Special care was taken to minimize pressure disturbances, as we were interested in measuring metastable films at low surfactant concentrations. A nanomover was used to drive a 20 ml gas-tight syringe and change the gas pressure in a TFB cell.

Foam/froth stability

The stability of three-dimensional foams was measured by the shake tests (20). The tests were conducted using 50 ml volumetric flasks filled with 25 ml of surfactant solution. Each solution was shaken by hand at fixed frequency and time, then left to stand. The decay time of the foam was recorded as the time it took for a clear surface to appear at the center of the foam.

The pressure decay method (PDM) was used to assess the stability of three-dimensional foams/froths in a more reproducible manner. The principle of this method is based on monitoring the increase in pressure in a froth chamber when bubbles rupture. In a closed foam column, the pressure inside rises as bubbles collapse as a result of bursting, coalescence, and/or diffusion. The change in pressure (ΔP) is directly related to the decrease in the bubble surface area (ΔA) as follows (21):

$$3V \cdot \Delta P + 2\gamma \cdot \Delta A = 0 \qquad [2.10]$$

where V is the total volume of the foam and the vapor space external to the foam, and γ is the surface tension.

A dimensionless fractional interfacial area at any given time t during foam decay was calculated by using the equation (22),

$$A / A_0 = (\Delta P_\infty - \Delta P_t) / \Delta P_\infty \qquad [2.11]$$

where A and A_0 are the instant and initial interfacial area of the foam, respectively, ΔP_t and ΔP_∞ are the instant and the final net pressure change, respectively. The rate of decrease in A/A_0 indicates the rate of collapse of the foam, thus the foam stability.

Similar to the device described by Murray and Liang (23), a reference chamber identical to the sample chamber was used to minimize the effect of temperature fluctuation on the differential pressure measurements. Nitrogen gas saturated with water was used to produce the foam, with a constant flow rate of 0.6 liter per minute. Nitrogen was bubbled through the sample solution via 12 stainless steel needles (inner diameter 0.1 mm) for 30±1 seconds before valves were closed and the pressure difference between the sample and reference chambers was subsequently monitored.

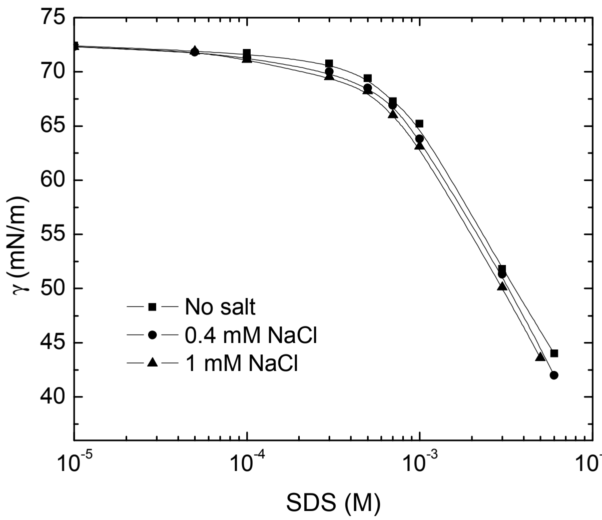

Figure 2.2 Surface tensions of SDS solutions in presence and absence of NaCl.

2.4 Results

Figure 2.2 shows the surface tension isotherms for the SDS solutions at 0, 0.4 and 1 mM NaCl. These salt concentrations were chosen for two reasons. First, the decrease in surface tension due to the presence of salt was discernable at 0.4 and 1 mM NaCl so that one can study the effect of NaCl on hydrophobic force. Second, the surface tension at 10^{-4} M SDS, at which concentration we planned to measure the contributions from hydrophobic force, was high enough to see hydrophobic effect. To date, the presence of hydrophobic forces in foam films have been reported at relatively low surfactant concentrations.

The surface excess of SDS was obtained using Eqs. [2.1] and [2.2] and is shown in Figure 2.3. The slope ($\partial\gamma/\partial \ln C_{SDS}$) of the surface tension isotherm were obtained by polynomial fit of the curves shown in Figure 2.2. As predicted by the Gouy-Chapman theory, added salt systematically promotes surfactant adsorption since salt can decrease the free energy of forming a charged monolayer with increasing ionic strength (13).

The Stern potentials (ψ_s) at the air/water interface were calculated using Eq. [2.8] and are given in Figure 2.4. As shown, ψ_s decreased systematically with increasing NaCl concentration, which may seem contradictory to what has been shown in Figure 2.3. However, added electrolytes increased the ionic strength and, thereby, caused a decrease in the Stern potential (see Eqs. [2.6] and [2.8]).

When SDS concentration became higher than the fixed NaCl concentrations, the three curves tend to overlap with each other. This can be attributed to the fact that the ionic strengths employed in the three sets of experiments were close to each other. Likewise, the sharp decrease in ψ_s above 10^{-3} M SDS can be attributed to the increase in ionic strength (21).

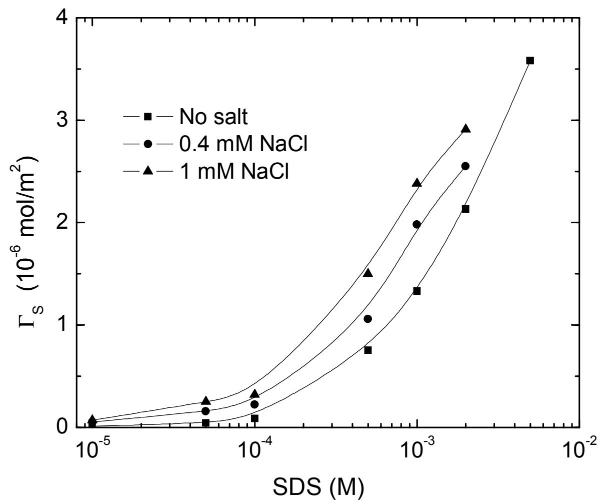

Figure 2.3 Adsorption isotherms for SDS as obtained using Eq. [2.1] and the surface tension data given in Figure 2.2.

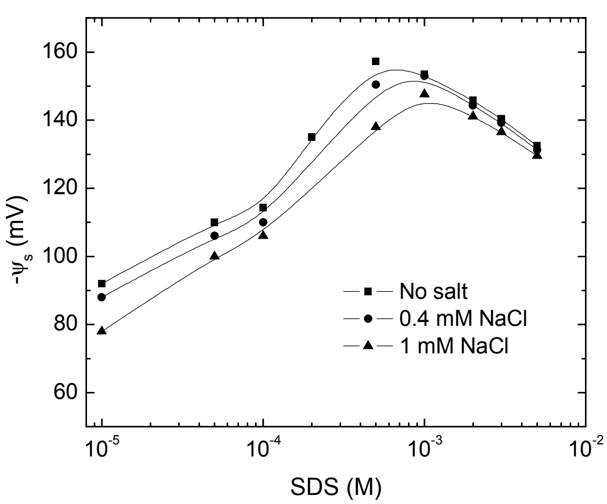

Figure 2.4 The Stern potential at the air-water interface as calculated using the counterion binding model developed in the present work.

The Stern potentials predicted from the present model are comparable to those of the Kalinin-Radke's model (24), as shown in Figure 2.5. The model predictions are also close to the potentials measured experimentally by Warszyski et al. (16) at low surfactant concentrations. This concentration regime ($C_{SDS} < 2\times10^{-4}$M) is of interest to us, as strong hydrophobic forces have been observed at low surfactant concentrations (9,10). The discrepancy between the Warszyski et al's experimental data (16) and the Stern potentials calculated using the Kalinin-Radke's (24) and present models may be due to the fact that the experimental measurements included the effects of the dipole moments of the hydrocarbon chain at the interface.

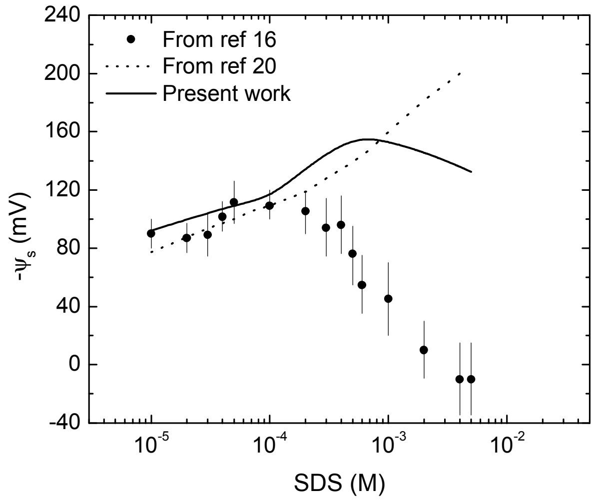

Figure 2.5. Comparison of the surface potentials predicted using the counterion binding models from ref (20) and the present work. The experimental data represent the surface potentials measured using the vibrating capacitor method (16).

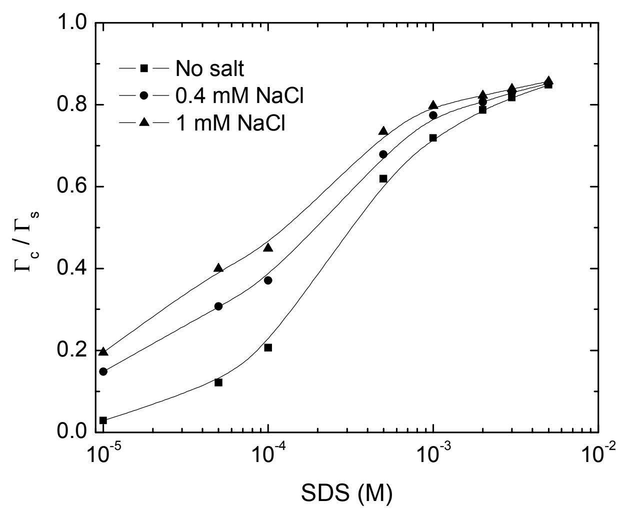

Figure 2.6 The surface excess ratio between the counterions (Na^+) and the surfactant ions (DS^-) as a function of SDS concentration in the presence and absence of NaCl.

Figure 2.6 shows plots of Γ_c / Γ_s representing the fraction of the DS^- ions bonded to Na^+ ions. Above cmc, the fractions were in the range of 0.85 to 0.9, which agrees well with the results of other authors (25-27). It is shown also that NaCl promotes counterion binding particularly at low surfactant concentrations. At concentrations above cmc, where the SDS concentration far exceeds that of NaCl, the effect of electrolyte is negligible.

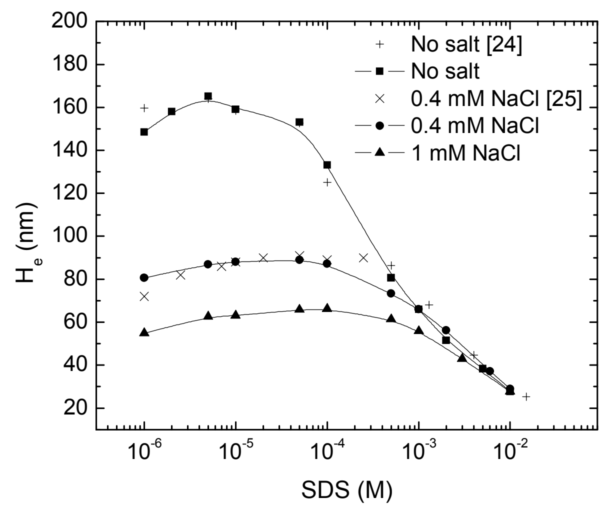

Figure 2.7 Equilibrium film thicknesses as a function of SDS concentration at 0, 0.4 and 1 mM NaCl; pH 5.7-6.0; and 25±0.1°C.

Figure 2.7 shows the equilibrium film thicknesses (H_e) measured at varying SDS concentrations both in the presence and absence of NaCl. As shown, H_e decreased sharply with increasing electrolyte concentration due to double layer compression. These results are in close agreement with those obtained in refs (28) and (29). In general, H_e decreased with increasing SDS concentration, which was also due to the double layer compression caused by the high ionic strengths created by the ionic surfactant itself. This decrease in H_e was observed despite the fact that Γ_s and, hence, $-\psi_s$ increased with increasing surfactant concentration as shown in Figure 2.3 and 2.4, respectively. Thus, there are two opposing causes in determining H_e, i.e., Stern potential and ionic strength, of which the latter has the overriding influence, particularly at high SDS concentrations.

Note, however, that H_e increased slightly as the SDS concentration increased from 10^{-6} to 4×10^{-6} M in the absence of NaCl. Likewise, H_e increased slightly as SDS concentration increased in the presence of NaCl. These increases were observed only at low surfactant concentrations before ionic strength became an overriding factor. Exerowa et al (29,30) also observed that H_e increases with increasing SDS concentration at 0.4 mM NaCl, as shown in Figure 2.7. These investigators attributed it to the increase in surface potential. The slight increase in H_e at low SDS concentration may also be due to a decrease in hydrophobic force with increasing SDS concentration. The presence of an attractive hydrophobic force should cause H_e to decrease. As will be shown later, the hydrophobic force decreases with increasing SDS concentration, which should cause H_e to increase. The hydrophobic force is strong at low surfactant concentrations, which is the reason that the slight increase in H_e with SDS concentration was observed only at low SDS concentrations.

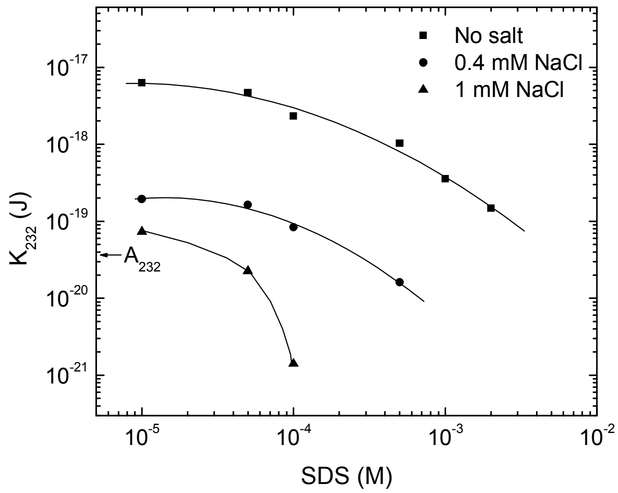

Figure 2.8 K_{232} in Eq. [2.14] as a function of SDS concentration at 0, 0.4 and 1 mM NaCl.

From the data presented heretofore, we can estimate the contributions from the hydrophobic force in the same manner as described by Yoon and Aksoy[9]. At equilibrium, the sum of the disjoining pressure (Π) in a soap film and the capillary pressure (P_c) should be the same. Thus,

$$\Pi - P_c = 0 \qquad [2.12]$$

According to the extended DLVO theory,

$$\Pi = \Pi_{el} + \Pi_{vw} + \Pi_{hb} \qquad [2.13]$$

where Π_{el}, Π_{vw}, and Π_{hb} represent contributions from electrostatic, van der Waals and hydrophobic forces, respectively. The first two contributions are well understood, while Π_{hb} can be given in single or double-exponential forms, or as a power law. Yoon and Aksoy used the following form (9):

$$\Pi_{hb} = -\frac{K_{232}}{6\pi H^3} \qquad [2.14]$$

where H is the distance between two charged surfaces and K_{232} is a hydrophobic force constant. An advantage of using Eq. [2.14] rather than an exponential form is that it is of the same form as the van der Waals' pressure. Therefore, K_{232} can be directly compared with the Hamaker constant A_{232}.

Substituting the expressions for Π_{el} and Π_{vw} that are commonly used for soap films, Eq. [2.11] becomes:

$$\Pi = 64(C_{SDS} + C_{NaCl})RT\tanh^2\left(\frac{ze\psi_s}{4kT}\right)\exp(-\kappa H) - \frac{A_{232}}{6\pi H^3} - \frac{K_{232}}{6\pi H^3} \qquad [2.15]$$

where A_{232} is the Hamaker constant for the foam film under consideration.

Substituting Eq. [2.15] into Eq. [2.12] which represents an equilibrium between the disjoining pressure and capillary pressure, we obtain:

$$64(C_{SDS} + C_{NaCl})RT\tanh^2\left(\frac{ze\psi_s}{4kT}\right)\exp(-\kappa H_e) - \frac{A_{232}}{6\pi H_e^{\,3}} - \frac{K_{232}}{6\pi H_e^{\,3}} - \frac{2\gamma}{r_c} = 0 \quad [2.16]$$

where r_c (=2.0 mm) is the radius of the ring cell. Note here that we use ψ_s calculated from Eq. [2.8] in calculating Π_{el} not to overestimate the contributions from Π_{hb}.

Equation [2.16] can now be used to obtain the values of K_{232} by substituting the values of H_e obtained at different C_{SDS} and C_{NaCl} (Figure 2.7); and by using the values of γ (Figure 2.2) and the value of A_{232}=3.7×10^{-20} J (15). The results are given in Table 1 and Figure 2.8 as functions of C_{SDS} and C_{NaCl}. In general, hydrophobic force decreases with increasing SDS and NaCl concentrations. Thus, air bubbles are most hydrophobic in pure water. As the SDS concentration increased, K_{232} decreased steadily. Note that at 5×10^{-3} M SDS and above, K_{232} became negative, indicating possibly the appearance of a repulsive force. This force may arise from the hydrated counter ions adsorbed on the polar heads of the DS^- ions.

NaCl addition reduced K_{232} by orders of magnitudes. It was reduced close to or below the value of A_{232} at 0.4 mM NaCl and above 5×10^{-4} M SDS. At a higher (1 mM) NaCl concentration, the same was observed at a 10-fold lower SDS concentration (5×10^{-5} M). Thus, electrolyte addition is an effective means of reducing the hydrophobic force in soap films. Similar observations were made in refs (9) and (10).

Table 2.1 The values of K_{232} of Eq. [2.14] at different SDS and NaCl concentrations.

SDS	NaCl		
(M)	0 mM	0.4 mM	1 mM
1×10^{-5}	6.27×10^{-18}	1.94×10^{-19}	7.31×10^{-20}
5×10^{-5}	4.68×10^{-18}	1.63×10^{-19}	2.25×10^{-20}
1×10^{-4}	2.33×10^{-18}	8.38×10^{-20}	1.41×10^{-21}
5×10^{-4}	1.03×10^{-18}	1.61×10^{-20}	-7.06×10^{-21}
1×10^{-3}	3.54×10^{-19}	-8.72×10^{-20}	-1.38×10^{-20}
2×10^{-3}	1.47×10^{-19}	-1.03×10^{-19}	-1.63×10^{-20}
5×10^{-3}	-1.70×10^{-21}	—	—
8×10^{-3}	-2.09×10^{-20}	—	—

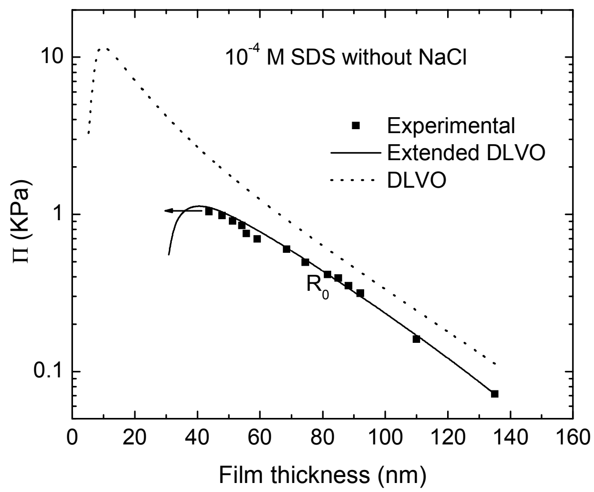

Figure 2.9 A disjoining pressure isotherm obtained at 0.1 mM SDS without NaCl. The solid line represents the extended-DLVO theory (Eq. [2.18] with ψ_s=-114.3 mV, K_{232}=2.33×10^{-18} J, A_{232}=3.7×10^{-20} J and κ^{-1}=30.4 nm. The dotted line represents Eq. [2 16] with K_{232} = 0. The arrow denotes typical rupture pressure, while R_0 represents the lowest rupture pressure observed.

In calculating K_{232}, as discussed above, knowing reliable values of ψ_s as functions C_{SDS} and C_{NaCl} is of critical importance. Figure 2.5 compares the Stern potentials derived from the counterion binding model developed in the present work and those of Kalinin-Radke (24). Also shown are the surface potentials measured by Warszyski et al (16). There are relatively small differences between the three sets of potentials at low SDS concentrations. It should be noted here that the K_{232} is not sensitive to the small differences between the Stern potentials calculated using the present model and the Kalinin-Radke's (24).

It is interesting that K_{232} changed its sign from positive (attractive) to negative (repulsive) at a critical concentration. The critical concentrations decreased with increasing NaCl concentration, i.e., ≥2×10^{-3} M SDS in the absence of NaCl, ≥1×10^{-3} M SDS at 0.4 mM NaCl, and ≥1×10^{-4} M SDS at 1 mM NaCl. These results indicate that combination of SDS and NaCl have compounded effects in decreasing hydrophobic force. In the vicinity of these critical concentrations, neither the hydrophobic force nor the hydration force is significant. Therefore, the DLVO theory would be valid at these concentrations.

A series of disjoining pressure isotherms were measured in the present work at 10^{-4} M SDS in the absence of NaCl. Figure 2.9 shows a typical isotherm. In this particular isotherm, the film ruptures at 43 nm and 1.1 kPa. The lowest rupture pressure recorded is denoted as R_0 in the figure. These rupture thicknesses were much larger than predicted by the DLVO theory, represented by the dotted line. Also, the measured pressures were considerably lower than predicted by the theory, indicating the presence of hydrophobic force. The discrepancy was much larger than observed with selfassembled monolayers of 12-cabon chain amines on mica[31], which seems to suggest that the hydrophobic force in soap films are larger and longer-ranged than observed with the amine-coated mica surfaces. The solid line in Figure 2.9 represents the extended DLVO theory (Eq. [2.18]), which includes contributions from the hydrophobic force. The extended DLVO fit was made with ψ_s =-114.3 mV, which was obtained from the counterion binding model derived in the present work and given in Figure 2.4; Debye lengths (κ^{-1}) of 30.4 nm; and K_{232}=2.33×10^{-18}, which was obtained from the values of H_e given in Table 2.1. The same values of ψ_s and κ^{-1} were used for the DLVO fit.

As the disjoining pressure was increased above 0.6 kPa, the film thicknesses fell into the regime of $\kappa H_e \leq 2$, in which case the weak overlap approximation for electrostatic force (Eqs. [2.15] and [2.16]) may not be applicable. We were, therefore, forced to calculate the following equation to obtain the full electrostatic contribution (12, 32):

$$\Pi_{el} = 2RTC_{el}\left(\cosh(\frac{e\psi_{mid}}{kT}) - 1\right) \qquad [2.17]$$

in which C_{el} =10^{-4} M SDS. The potential at the mid-plane of the film (ψ_{mid}) was calculated by numerically solving the full nonlinear Poisson-Boltzmann equation with constant-charge boundary conditions. In using Eq. [2.15], we assumed that the two air-water interfaces interacted under constant surface potential condition since it approximates the constant chemical potential condition rather well (33). We used the computer program given in ref (32). Thus, the extended DLVO fit given in Figure 2.9 is given by the following relationship:

$$\Pi = 2RTC_{el}\left(\cosh(\frac{e\psi_{mid}}{KT}) - 1\right) - \frac{A_{232}}{6\pi H_e^{\ 3}} - \frac{K_{232}}{6\pi H_e^{\ 3}} \qquad [2.18]$$

One can see that there is an excellent fit between the experiment and the extended DLVO theory.

Disjoining pressure measurements were also conducted at 10^{-4} M SDS in the presence of 0.4 and 1 mM NaCl. The results are given in Figure 2.10 along with the data obtained in the absence of NaCl for comparison. For the data obtained in the presence of NaCl, Eq. [2.13] rather than Eq. [2.16] was used for the DLVO and extended DLVO fits, since the weak overlap approximation of electrostatic force holds here. The results show that as the NaCl concentration increased, the films became thinner due to double layer compression, and yet the film became more stable. The increased stability may be due to the decreasing hydrophobic force with increasing NaCl concentration. At higher SDS and NaCl concentrations, hydration force may also stabilize the film.

The disjoining pressure isotherm obtained at 0.4 mM NaCl and given in Figure 2.10 shows a rupture pressure of 6.0 kPa. In some other measurements conducted at the same NaCl and SDS concentrations, the rupture pressure was as low as 0.9 kPa, as indicated by R_{01}. The isotherm obtained at 1 mM NaCl, on the other hand, shows no rupture at a pressure at 8.5 kPa, which was the highest pressure attainable with the apparatus we used.

As has already been noted, the disjoining pressure isotherm obtained at 10^{-4} M SDS in the absence of NaCl shows a large discrepancy between the experiment and DLVO theory. The discrepancy is still discernable at 0.4 mM NaCl, but the data obtained at 1 mM NaCl exhibited a reasonable fit with the classical DLVO theory. The decreasing discrepancy between the theory and experiment can be attributed to the diminishing hydrophobic force with increasing NaCl concentration.

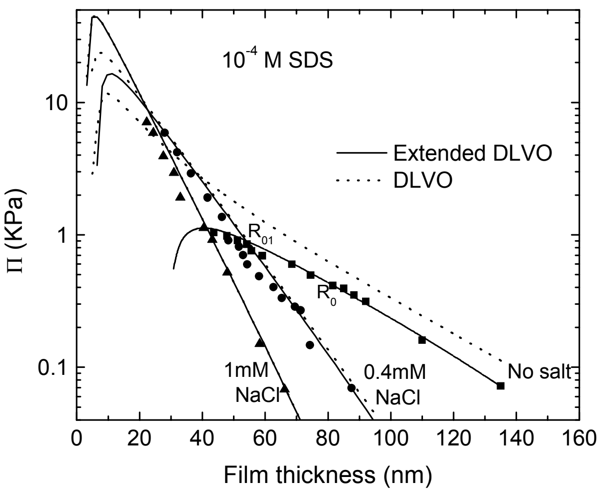

Figure 2.10 Disjoining pressure isotherms obtained in 10^{-4} SDS solutions at different NaCl additions. The solid lines represent Eq. [2.18] with ψ_s =-114.3 mV, K_{232}=2.33×10^{-18} J, κ^{-1} =30.4 nm, 0 mM NaCl; Eq. [2.15] with ψ_s =-110.0 mV, K_{232}=8.38×10^{-20} J, κ^{-1}=13.6 nm, 0.4 mM NaCl; Eq. [2.15] with ψ_s =-106.4 mV, K_{232}=1.41×10^{-21} J, κ^{-1}=9.2 nm, 1 mM NaCl. The dotted lines represent Eqs. [2.16] and [2.13] with K_{232}=0.

Figure 2.10 clearly shows the effect of double-layer compression as indicated by the sharp increase on the slopes of the isotherms. According to the theoretical fits given in Figure 2.10, the Debye length decreased from 30.4, 13.6 and 9.2 nm as the salt concentration was increased from 0, 0.4 and 1 mM, respectively.

2.5 Discussion

From the disjoining pressure isotherms (Figure 2.9 and 2.10), it would be natural to think that foam stability is related to the rupture pressure of foam films. Foam stability is frequently measured by simple shaking tests (20). For the solutions containing 10^{-4} M SDS, the lifetime of foam (τ) increased with increasing NaCl addition. As NaCl concentration was increased from 0, 0.4 and 1 mM NaCl, τ increased from 32, 89, and 162 s, respectively. We believe that the increase in foam stability is at least partially due to the rapid decrease in hydrophobic force in foam films. When the NaCl concentration was increased further, it was found that τ began to decrease. At 10 mM NaCl, τ decreased to 128 s, and at 100 mM NaCl it decreased further to 65 s. The decrease in foam lifetime at such high NaCl concentrations was most likely due to the decrease in electrostatic repulsion in foam films.

The pressure decay method was employed to assess foam stability more exactly and reproducibly. Figure 2.11 shows that the foam produced at 10^{-4} M SDS with no added NaCl was unstable and its stability decayed in several seconds. When 0.001 M NaCl was added, the rate of decay in interfacial area of the foam was much lower, indicating that the stability of the foam is improved by adding moderate amount of electrolyte. At 0.1 M NaCl, however, the decay curve shifted back to the left and became steeper, indicating that addition of high concentration electrolyte destabilizes the foam.

In the present work, the disjoining pressure isotherms were fitted to the DLVO theory, as many other investigators did, to back calculate the surface potentials. At 10^{-4} M SDS in the absence of NaCl, we obtained the value of ψ_s =-74.4 mV, which was approximately 40 mV less negative than those reported in the literature (16, 20). Furthermore, the DLVO theory predicted the primary maximum to occur at 15 nm, while it was observed at 40 nm in experiment. This discrepancy indicates the presence of a strong attractive force not considered in the DLVO theory. Bergeron[31] reported a disjoining pressure isotherm at 10^{-3} M SDS. Even at such a high surfactant concentration, the author suggested the presence of an attractive force larger than the van der Waals force.

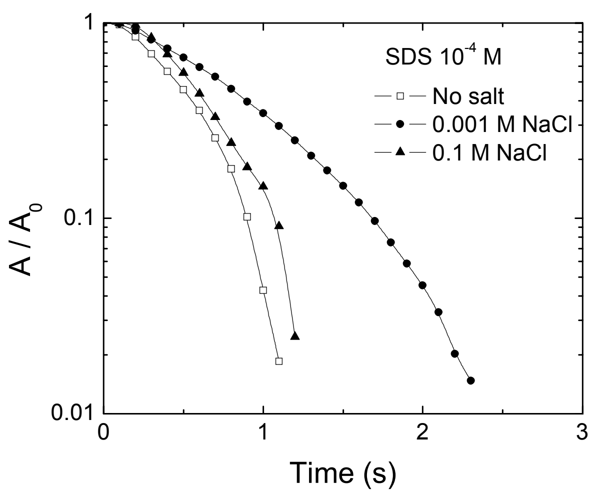

Figure 2.11 Surface area decay of SDS foams containing various concentrations of NaCl.

In general, the hydrophobicity of a surface and, hence, its hydrophobic force is controlled by changes in surface composition. Likewise, the decrease in hydrophobic force in the presence of electrolytes may be due to the adsorption of the ions on the surface (10,32). Figure 2.12 shows plots of K_{232} vs. the surface coverage (θ) of the surfactant ions at the air/water interface. The surface coverage may be given by

$$\theta = \Gamma_s / \Gamma_{\max}, \qquad [2.19]$$

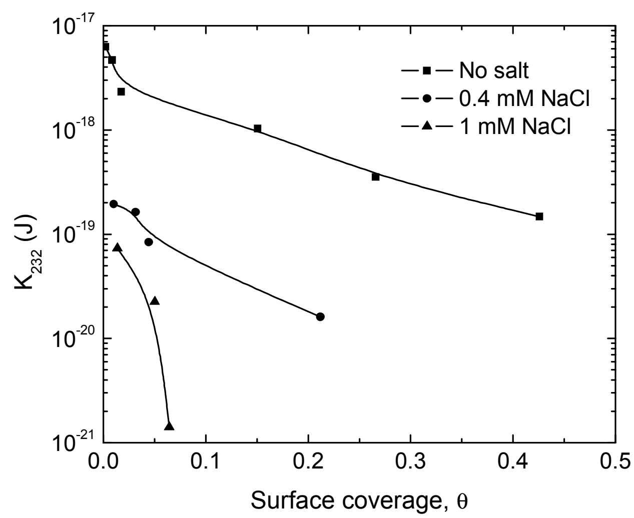

Figure 2.12 K_{232} of Eq. [2.14] as a function of the fraction of the air/water interface covered by SDS.

where Γ_{max} is set to be 5×10^{-6} mol/m^2 from the surface tension measurement. K_{232} decreases with increasing θ, which appears to support the finding that surfactant adsorbing at the air/water interface renders the surface hydrophilic. The data given in Figure 2.12, on the other hand, show that K_{232} decreases with increasing NaCl concentration. This finding suggests that the adsorption of the electrolyte (anion, cation or both) may responsible for the decrease in hydrophobic force. Another possible reason may be that the electrolyte may change the water structure and decrease the hydrophobic force, as will be further discussed later.

Thus, the data presented in the present work suggest that the hydrophobic force in thin aqueous films is maximum in the absence of any surfactant or electrolyte. This is not surprising from a thermodynamic point of view, as surfactant addition causes surfacetension to decrease. On the other hand, the results are surprising with regard to the role of electrolyte, as addition of inorganic electrolytes to pure water causes its surface tension to increase. Although the adsorption of ionic surfactants is promoted in the presence of electrolytes, it is not the primary reason causing a decrease in hydrophobic force. Electrolyte itself may have a profound impact on the hydrophobic forces between two air bubbles, as suggested by Craig et al (7).

While the nature of hydrophobic force and its very existence are in debate, the nature of hydrophobic effect is well understood (33,34). Two hydrophobic substances such as hydrocarbon chains in water are attracted to each other because the cohesive energy between water molecules is much stronger than the interaction energy between the hydrophobic substance and water. As a consequence, the hydrophobic substances are pushed toward each other by surrounding water molecules, which may be manifested as attractive hydrophobic force. What is in question, however, is the range of separation distances over which the hydrophobic forces are operating. When hydrocarbon chains are interacting with each other in water, the distance range may be short. It has been shown, on the other hand, that macroscopic hydrophobic particles are brought together in water, which is a phenomenon known as hydrophobic coagulation. It has been shown that the attractive forces are much larger than the van der Waals force, and the kinetics of coagulation increases with increasing particle hydrophobicity (35). Recognizing that these particles are in the range of tens of microns, the surface forces operating between them may be much longer-ranged than those between hydrocarbon chains in water. In this regard, the hydrophobic forces observed in thin aqueous films may originate from the large cohesive energy of water. The stronger the cohesive energy is, the stronger the hydrophobic force should become. That we have observed the strongest hydrophobic force in the absence of any surfactant or electrolyte may be attributed to the large cohesive energy of water (102 mJ/m^2). In the presence of electrolyte, the cohesive energy may be substantially compromised, causing a decrease in hydrophobic force. The Na^+ and Cl^- ions used in the present work may disrupt the hydrogen bonding net work in water, reduce its cohesive energy, and cause a decrease in hydrophobic force. By virtue of its small ionic size, Na^+ ions may be particularly disruptive of the water structure. Liu, et al (36) used the vibrational sum frequency generation spectroscopy (SFG) to characterize the air/water interface. However, they detected little changes at the interface at 1.0 M NaCl. It would, therefore, be likely that NaCl affects the structure of bulk water and affect the hydrophobic force.

The bubble coalescence studies conducted by Criag el at (7) showed that air bubbles are most unstable in the absence of electrolyte, and suggested that the instability arises from hydrophobic force. The bubbles become increasingly stable as electrolyte concentration is increased. However, the changes in stability was not discernable until NaCl concentration reached 2×10^{-3} M, which suggested that the hydrophobic force is not mitigated by the electrolyte up to this concentration. In the present work, however, the hydrophobic force was substantially reduced at 4×10^{-4} M, indicating that the technique (i.e., equilibrium film thickness measurement) employed in the present work is far more sensitive than the bubble coalescence method.

Angarska et al (10) measured the critical rupture thickness and measured the long-range hydrophobic forces with decay length (λ) of 15.8 nm at 3×10^{-1} M NaCl and various SDS concentrations. At 10^{-5} M SDS, the value of the pre-exponential parameter (B) of the exponential force law was 3.34×10^{-5} mN/m, which was exceedingly small as compared to those reported in the literature for the hydrophobic forces measured with solid surfaces. Typically, the values of B for the long-range hydrophobic forces are in the range of 0.1 to 2 mN/m. Thus, the hydrophobic forces measured by Angarska et al. at the high electrolyte concentration is rather weak, as has been found in the present work.

2.6 Conclusions

The presence of NaCl in SDS solutions enhances the surfactant adsorption at the air/water interface. However, it causes a decrease in the Stern potentials due to double-layer compression. The TFB studies conducted on the system showed that equilibrium film thickness decreases with increasing NaCl concentration, which is due to the decrease in the Stern potential and Debye length.

The equilibrium film thicknesses measured and the Stern potentials calculated from a counterion binding model were used to estimate the magnitudes of the hydrophobic forces in the thin aqueous films. It was found that the hydrophobic force decreases sharply with increasing SDS and NaCl concentrations.

Disjoining pressure isotherms were obtained using the TFB technique. The isotherms obtained at 10^{-4} M SDS showed that NaCl additions cause films to become thinner due to double-layer compression and cause the film rupture pressures to increase. The disjoining pressure isotherms were fitted to the extended DLVO theory, with the hydrophobic force constants determined from the equilibrium film thickness measurements. There was an excellent fit between the theory and experiment, which supports the presence of hydrophobic forces in thin aqueous films.

The shake tests conducted in the present work showed that foam stability increases with increasing NaCl concentration, which was in agreement with the findings of the disjoining pressure isotherms. The increase in foam stability can be attributed to the decrease in hydrophobic force with increasing electrolyte concentrations, which in turn may be ascribed to the decrease in the cohesive energy of water in the presence of the electrolyte.

2.7 References

1. Scheludko A.; Exerowa, D. *Kolloid Z.* 165 (1959)148.
2. Mysels, K.J. *J. Phs. Chem.* 68 (1964) 3441.
3. Mysels, K. J.; Jones, M.N. *Disc. Far. Soc*. 42 (1966) 42.
4. Derjaguin, B.V.; Landau, L. *Acta Physicochim. U.R.S.S.* 14 (1941) 633.
5. Verwey, E.J.W.; Overbeek, J.T.G. *Theory of the Stability of Lyophobic Colloids*; Elsevier: Amsterdam, 1948.
6. Yoon, R.-H.; Yordan, J. L. *J. Colloid Interface Sci.* 146 (1991) 565
7. Craig, V.S.J.; Ninham, B.W.; Pashley, R.M. *J. Phys. Chem.* 97 (1993) 10192.
8. Deschenes, L.; Zilaro, A. P.; Muller, L.J.; Fourkas, J.T.; Mohanty, U. *J. Phys. Chem.* 101 (1997) 5777.
9. Yoon, R.-H.; Aksoy, B.S. *J. Colloid Interface Sci.* 211 (1999) 1.
10. Angarska, J.K.; Dimitrova, B.S.; Danov, K.D.; Kralchevsky, P.A.; Ananthapadmanabhan, K.P.; Lips, A. *Langmuir* 20 (2004) 1799.
11. Krustev, R.; Müller, H.J. *Langmuir* 15 (1999) 2134.
12. Yaros, H. D.; Newman, J.; Radke, C. J. *J. Colloid and Interface Sci.* 262 (2003) 442.
13. Persson, C.; Jonsson, A.; Bergstrom, M.; Eriksson, J.C. *Journal of Colloid and Interface Sci.* 267 (2003) 151.
14. Tchaliovska, S.; Manev, E.; Radoev, B.; Eriksson, J. C.; Claesson, P. M. *J. Colloid Interface Sci.* 168 (1994) 190.

15. Israelachvili, J. N. *Intermolecular and Surface Forces*; Academic press: London, 1992.
16. Warszynski, P.; Barzyk, W.; Lunkenheimer, K.; Fruhner, H. *J. Phys. Chem. B* 102 (1998) 10948.
17. Adamson, A.W. *Physical Chemistry of Surfaces*; John Wiley & Sons, Inc., 1990.
18. Cascão Pereira, L.G.; Johansson, C.; Blanch, H.W.; Radke, C.J. *Colloids and Surfaces, A.* 186 (2001) 103.
19. Bergeron V.; Radke, C.J. *Langmuir* 8 (1992) 3020.
20. Waltermo, A.; Claesson, P. M.; Simonsson, S.; Manev, E.; Johansson I.; Bergeron, V. *Langmuir* 12 (1996) 5271.
21. Nishioka, G., and Ross, S., *J Colloid Interface Sci*, 81 (1981) 1.
22. Yu, M –A, and Damodaran, S., *J Agric Food Chem,*39 (1991) 1555.
23. Murray, B S, and Liang, H.-J., *J Agric Food Chem,* 47 (1999) 4984.
24. Kalinin, V.V.; Radke, C.J., *Colloids and Surfaces, A* 114 (1996) 337.
25. Kralchevsky, P.A.; Danov, K.D.; Broze, G.; Mehreteab, A. *Langmuir* 15 (1999) 2351
26. Cross, A.W.; Jayson, G.G. *J. Colloid Interface Sci.* 162 (1994) 45.
27. Johnson, S.B.; Drummond, C.M.; Scales, P.J.; Nishimura, S. *Langmuir*11 (1995) 2367.
28. Aksoy, B.S. *PhD Thesis*, Virginia Polytechnic Institute and State University, 1997.
29. Exerowa, D.; Zacharieva, M.; Cohen R.; Platikanov, D. *Colloid & Polymer Sci.* 257 (1979) 1089.
30. Exerowa, D.; Kruglyakov, P. M. *Foam and Foam Films*; Elsevier: Amsterdam, 1998.
31. Yoon, R.-H.; Ravishankar, S.A. *J. Colloid Interface Sci.* 179 (1996) 403.
32. Yaros, H. D. *PhD thesis*, University of California at Berkeley, 2002.
33. Eriksson, J.C.; Ljunggren, S. *Progr Colloid Polym Sci.* 76 (1988) 188.
34. Bergeron, V. *PhD thesis*, University of California at Berkeley, 1993
35. Christenson, H.K.; Claesson, P.M.; Berg, J.; Herder, P.C. *J. Phys. Chem.* 93 (1989) 1472.
36. Tanford, C. *The Hydrophobic Effect: Formation of Micelles and Biological Membranes;* Wiley: New York, 1973.
37. Van Oss, C.J. *Interfacial Forces in Aqueous Media*; Marcel Dekker: New York, 1994.
38. Xu, Z.; Yoon, R.-H. *J. Colloid Interface Sci.* 134 (1990) 427.
39. Liu, D.; Ma, G.; Levering, L.M.; Allen, H. C. *J. Phys. Chem. B.* 108 (2004) 2252.

Appendix 2A

Thin Film Pressure Balance Technique

2A.1 Film Thickness Measurement

Figure 2A.1 demonstrated the schematic diagram of the Scheludko Cell, which is essentially a glass capillary tube with a small orifice connecting a side glass tube. The side glass tube is used to transport solution (or water). A single horizontal foam film is formed by sucking out the aqueous solution in a Scheludko Cell. Prior to experiments, it is important to make the inner wall of the film holder hydrophilic. Therefore, much effort should be made to clean the film holder.

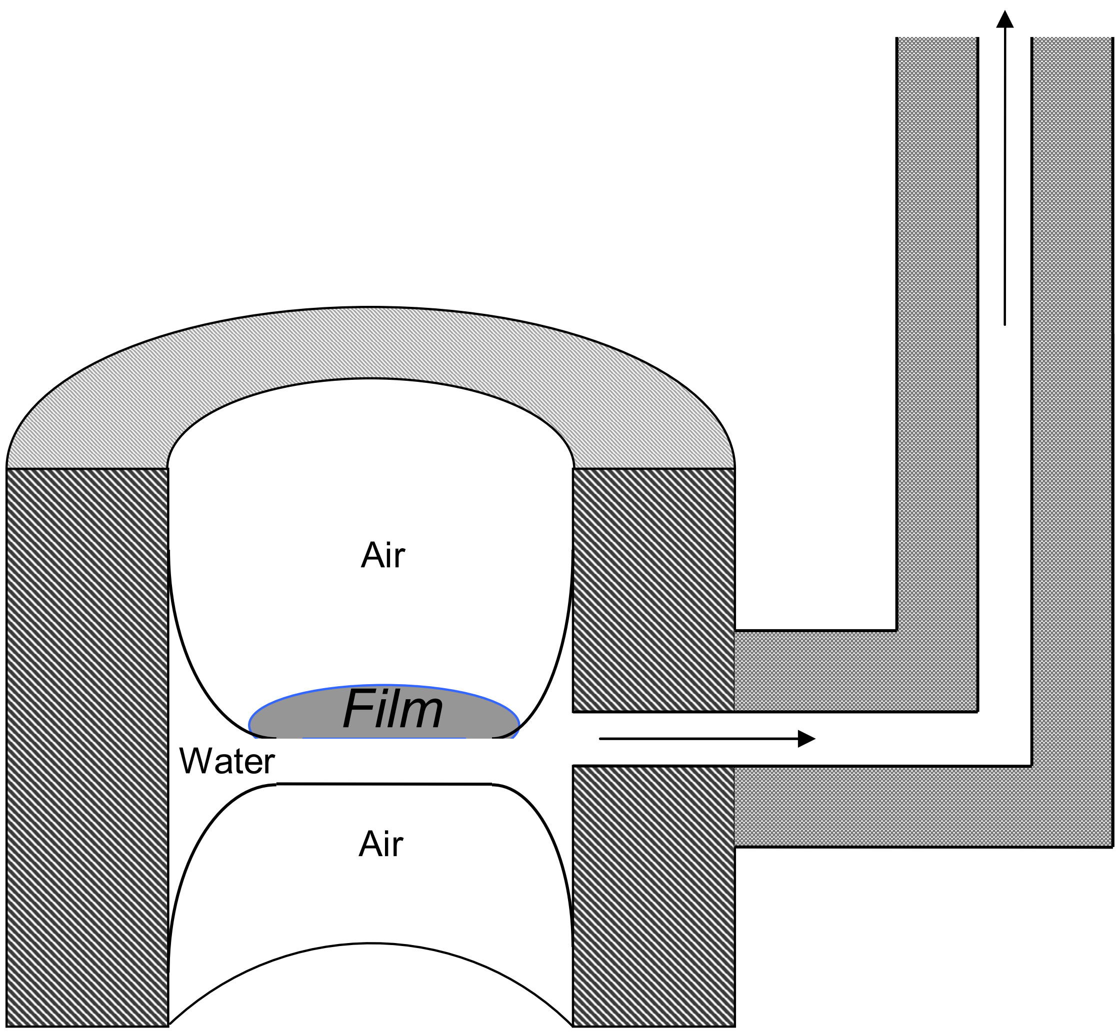

Figure 2A.1 Schematic diagram of the Scheludko cell.

Film thickness can be determined using thin-film interferometry. Figure 2A.2a represents the principle of this measurement. The two set of light waves, reflected from the bottom surface and the upper surface of the film, respectively, interfere with each other. The optical path differences between the interfering waves generate a phase difference that can be used to extract the film thickness.

For a normal incidence light of wave length (λ), and a homogeneous film with a refractive index (n_f), the optical path difference is $\lambda/2$ between the incidence light and what is reflected from the bottom surface of the film; the optical path difference is $2n_f$H between the incidence light and what is reflected from the upper surface of the film. The sum of the path differences of above-mentioned two determines the total intensity of the reflected light. The following equation gives the equivalent thickness (H) of the foam film (30):

$$H = \frac{\lambda}{2\pi n_f} \arcsin \sqrt{\frac{\Delta}{1 + \frac{4R(1-\Delta)}{(1-R)^2}}} \qquad [2A.1]$$

where

$$R = \left(\frac{n_f - 1}{n_f + 1} \right)^2, n_f = 1.33$$

and

$$\Delta = (I - I_{\min}) / (I_{\max} - I_{\min}).$$

In the above equation, $I_{\max}$ and $I_{\min}$ is respectively the last maximum and minimum intensities of the reflected light from the film, while I is the intensity during the thinning of the film. Figure 2A.2b is a typical diagram that shows the reflected light intensity a foam film changes with time. Using Eqs. [2A.1], one can convert the reflectance vs. time curve to film thickness vs. time curve. The latter can be used to study the kinetics of film thinning. At the final stage of film thinning, the light intensity levels out, indicating that the film approaches the equilibrium state.

The equivalent thickness (H) should be corrected for the two hydrocarbon surface layers whose refractive index is considered to be higher than that of water. According to Ref. (34), a reasonable estimate for the total thickness (h_{surf}) of the surfactant layers is less than 2 nm, especially when the surfactant concentrations are low in our case. In fact, h_{surf} is much smaller than the thicknesses measured in this work and is therefore neglected.

Figure 2A.3 compares the equilibrium thickness measurements for SDS-stabilized foam films formed in the Scheludko cell of 4 mm inner diameter. Although the experiments have been conducted at different time and place, the agreement of the results is remarkable.

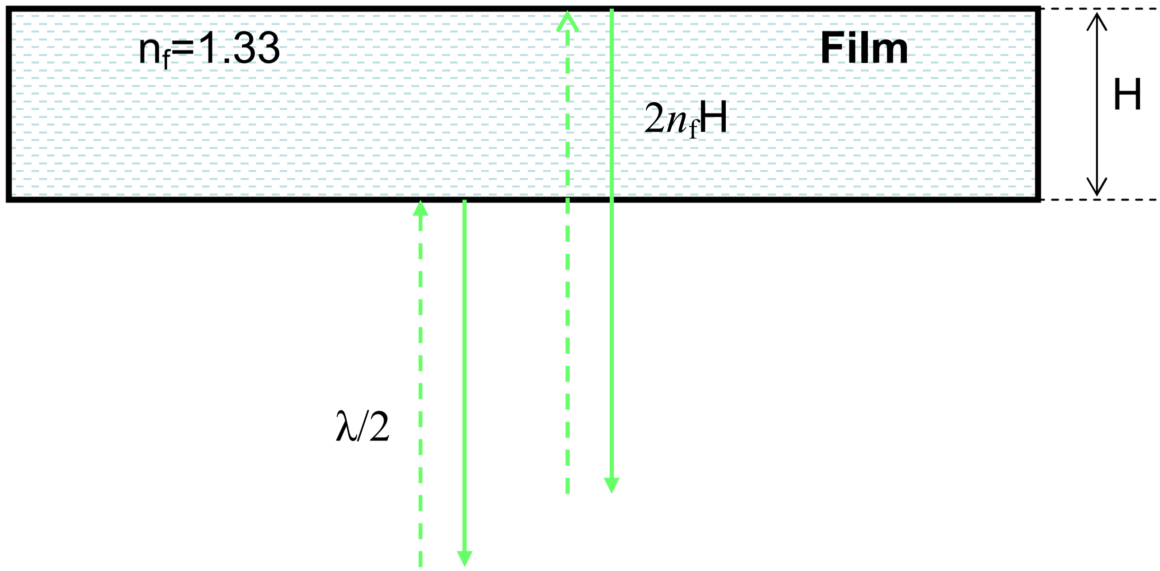

a)

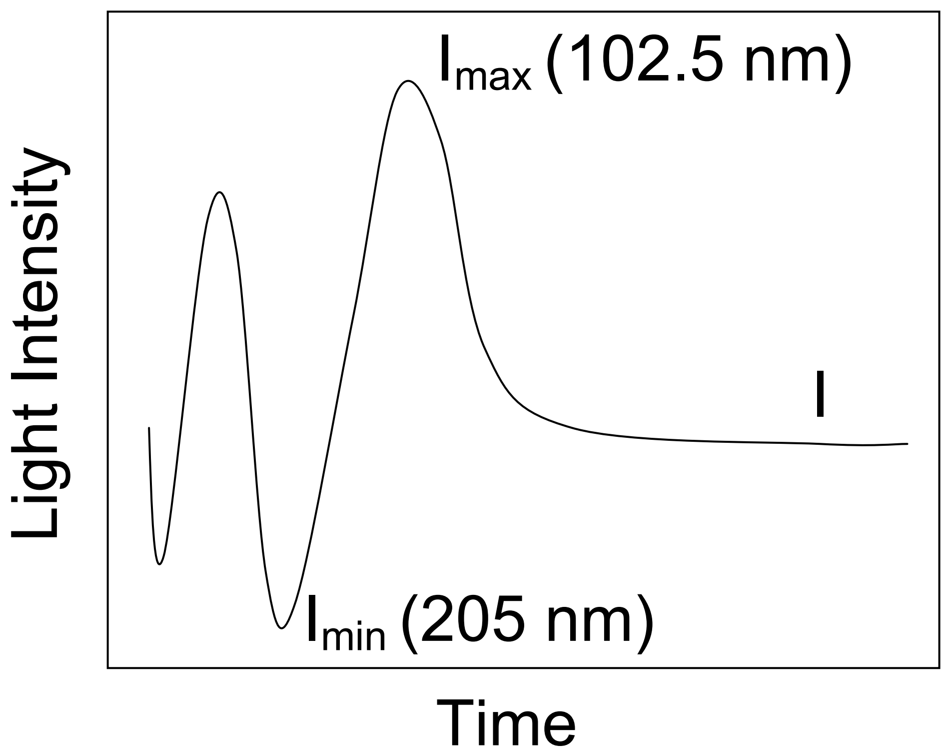

b)

Figure 2A.2 The intensity of light reflected from the two air/water interfaces of a foam film changes with time.

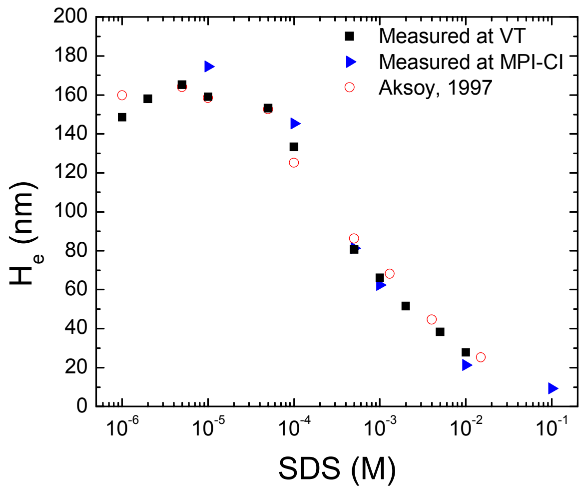

Figure 2A.3 Equilibrium film thicknesses (H_e) versus SDS concentration. The squares represent H_e measured using the new thin film pressure balance at Virginia Tech (VT); the triangles represent H_e measured at Max Planck Institute of Colloids and Interfaces (MPI-CI) in Germany; the circles represent the work of Aksoy's (28).

2A.2. Disjoining Pressure Measurement

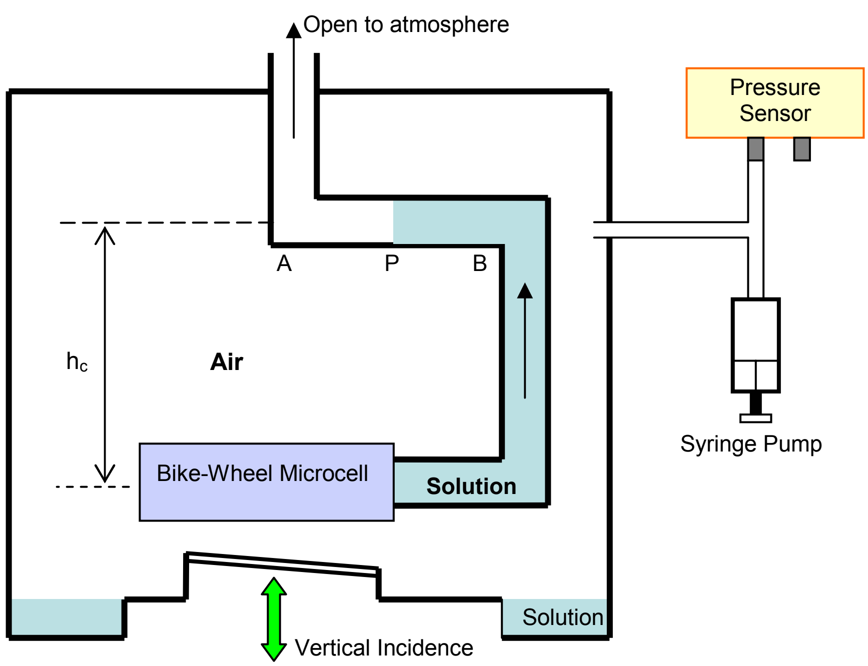

Figure 2A.4 Schematic of the experimental apparatus for measuring disjoining pressure isotherm. The forefront (P) of the solution moving along the horizontal part (AB) of the capillary tube as air pressure is changed. The thin film is formed inside the orifice (the hub), which is connected to the annulus (the wheel) *via* the spoke channels. More detailed information on the bike-wheel microcell is given by Cascão Pereira et al (18).

Appendix 2B

Three-Dimensional Foam Stability Measurement

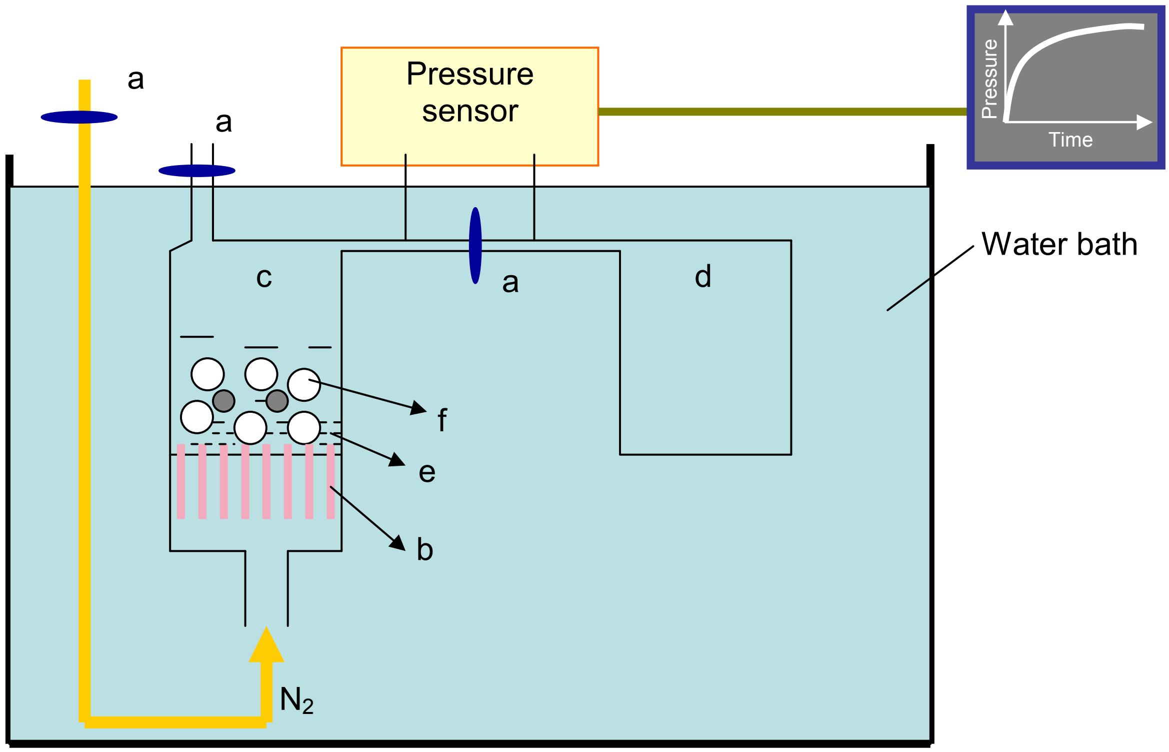

Figure 2B.1 Schematic drawing of pressure decay method. Valves (a), 12 stainless steel needles with I.D. of 0.1 mm (b), cylindrical glass sample chamber (c), cylindrical glass reference chamber (d), surfactant solution in sample chamber (e), foams or froths (f).